Pergamon

Acta mater. Vol. 45, No. 11, pp. 4797–4806, 1997

Printed in Great Britain
PII: S1359-6454(97)00132-8
1359-6454/97 $17.00 + 0.00

CREEP BEHAVIOR OF AN Al-6061 METAL MATRIX COMPOSITE REINFORCED WITH ALUMINA PARTICULATES

YONG LI and TERENCE G. LANGDON

Departments of Materials Science and Mechanical Engineering, University of Southern California, Los Angeles, CA 90089-1453, U.S.A.

(Received 20 January 1997)

Abstract—Creep tests were conducted on an Al-6061 matrix alloy reinforced with 20 vol.% of irregularly shaped Al_2O_3 particulates. The composite was fabricated using an ingot metallurgy technique and the creep properties were determined at temperatures from 623 to 773 K. The results show high values for both the apparent stress exponent (up to > 10) and the apparent activation energy for creep ($\sim$ 200–275 kJ/mol) but it is demonstrated, by incorporating a threshold stress into the analysis, that the true stress exponent is close to 3 and the true activation energy is close to the value for diffusion of Mg in the Al matrix. The results suggest that creep is controlled by the viscous glide of dislocations in the Al-6061 matrix alloy. Very fast creep rates are observed at the highest stress levels owing to the breakaway of dislocations from their solute atom atmospheres. Direct comparison shows that the creep resistance of this composite is less than in an Al-6061 alloy reinforced with 20 vol.% of Al_2O_3 microspheres. This difference is attributed to the creation of additional precipitates in the microsphere-reinforced composite because of an interfacial reaction between the matrix alloy and the reinforcement. © *1997 Acta Metallurgica Inc.*

1. INTRODUCTION

Earlier reports described the creep behavior of an Al-6061 metal matrix composite reinforced with 20 vol.% of Al_2O_3 microspheres and manufactured using a liquid metallurgy technique (herein designated Al 6061–20 vol.% Al_2O_3(s) where s denotes microspheres) [1, 2]. A unique feature of this composite was the introduction of a reinforcement of essentially spherical alumina-based microspheres consisting of a submicrometer mixture of alumina (α-Al_2O_3) and mullite ($3Al_2O_3 \cdot 2SiO_2$) and with the microspheres having a size range from ~ 5 to ~ 30 μm with an average diameter of ~ 20 μm. A liquid metallurgy processing route was developed in which preheated microspheres were added to a melt of the Al-6061 matrix alloy and the melt was cast into billets [3]. The experimental creep data from this composite showed that there was no true steady-state behavior but rather there was a short primary stage in which the strain rate dropped significantly and then there was a brief minimum creep rate prior to an extended tertiary stage. It was demonstrated also that the creep resistance of the composite was always higher than for the unreinforced monolithic Al-6061 matrix alloy under identical testing conditions.

There is evidence that the strengthening effect observed in metal matrix composites at low temperatures may be attributed, at least in part, to the additional dislocations introduced into the composites as a result of the mismatch in the values of the coefficients for thermal expansion (CTE) between the rigid ceramic reinforcement and the relatively soft metal matrix [4–8], and there is experimental evidence that the shape and geometry of the reinforcement may play an important role in the generation of dislocations due to this CTE mismatch [9]. The significance of reinforcement geometry under creep conditions may be demonstrated by noting that, in a direct comparison of the creep properties of whisker- and particulates-reinforced Al-6061 alloys, it was shown that whisker reinforcement is significantly more effective than particulates reinforcement in introducing creep resistance [10]. Thus, the reinforcement geometry appears to be an important, but relatively neglected, parameter.

Most of the creep investigations reported to date have been conducted on composites fabricated by powder metallurgy techniques [10–16] and there is only a small number of reports on composites fabricated using liquid metallurgy procedures [1, 2, 17, 18]. Furthermore, there has been no direct evaluation of the influence of reinforcement geometry on the creep properties of metal matrix composites prepared using liquid metallurgy techniques. The present investigation was therefore motivated by this apparent deficiency. Creep tests were conducted on an Al-6061 metal matrix composite manufactured by an ingot metallurgy technique and containing 20 vol.% of irregularly shaped Al_2O_3 particulates (hereafter designated Al 6061–20 vol.% Al_2O_3(p) where p denotes particulates). The creep tests were performed at temperatures from 623 to 773 K and over a range of strain rates covering up to five orders

of magnitude. This paper describes the results of this investigation and compares the creep data with the results obtained earlier from the Al-6061 alloy reinforced with spherical Al_2O_3 microspheres [2].

2. EXPERIMENTAL MATERIAL AND PROCEDURES

The metal matrix composite tested in the present investigation, Al 6061–20 vol.% Al_2O_3(p), was fabricated by a proprietary casting technique and contained 20 vol.% of irregularly shaped Al_2O_3 particulates. The material was received from Duralcan USA (San Diego, California) in the form of 19.1-mm diameter rods. According to information provided by the manufacturer, the Al_2O_3 particulates used in the processing were in the size range from ~ 16 to ~ 23 μm and with an average size of ~ 20 μm.

Specimens were machined from the rods for testing under double-shear conditions [19] using the same specimen configuration as in the report by Murty *et al.* [20]. Prior to testing, all specimens were subjected to a T6 heat treatment by solution treating at 803 K for 1.5 h, water quenching, holding at room temperature for 20 h and then ageing at 448 K for 8 h. Figure 1 gives a photomicrograph of the morphology of the Al_2O_3 particulates and the grain structure of the composite after the T6 heat treatment. Inspection of Fig. 1 shows that the distribution of alumina particles is reasonably uniform throughout the Al-6061 matrix and the grains are essentially equiaxed in shape. The mean linear intercept grain size was estimated as ~ 23 μm.

Creep tests were conducted in air under conditions of constant stress with the testing temperature continuously monitored and controlled to within ± 2 K of the desired value. The strain during creep was measured with a linear variable differential transformer (LVDT) and amplifier and it was continuously recorded on a strip chart recorder. Creep rates were recorded over a range of more than five orders of magnitude.

3. EXPERIMENTAL RESULTS

3.1. Creep curves

Representative creep curves are shown in Fig. 2 in a plot of shear strain, γ, vs time, t, for an absolute testing temperature, T, of 673 K. These curves exhibit a short primary stage, a very brief secondary stage where the creep rate is a minimum and then an extended tertiary stage. The general characteristics of the creep curves are similar to those for Al 6061–20 vol.% Al_2O_3(s) [2] and an Al–Mg composite reinforced with 26 vol.% of Al_2O_3 fibers [18]. The creep data for the three specimens of Fig. 2 are replotted in Fig. 3 as shear strain rate, $\dot{\gamma}$, vs shear strain, γ, and it is apparent that there is a brief minimum in the creep rate followed by a very extensive tertiary stage.

3.2. Stress and temperature dependence of the minimum creep rate

Tests were conducted at temperatures from 623 to 773 K and for each test the minimum strain rate, $\dot{\gamma}$, was plotted logarithmically against the shear stress, τ, as shown in Fig. 4.

Inspection of the results presented in Fig. 4 leads to several conclusions. First, the data appear to divide into two regions: there is a region I (representing all of the datum points at 773 K and the

Fig. 1. Microstructure of the Al 6061–20 vol.% Al_2O_3(p) composite after T6 heat treatment.

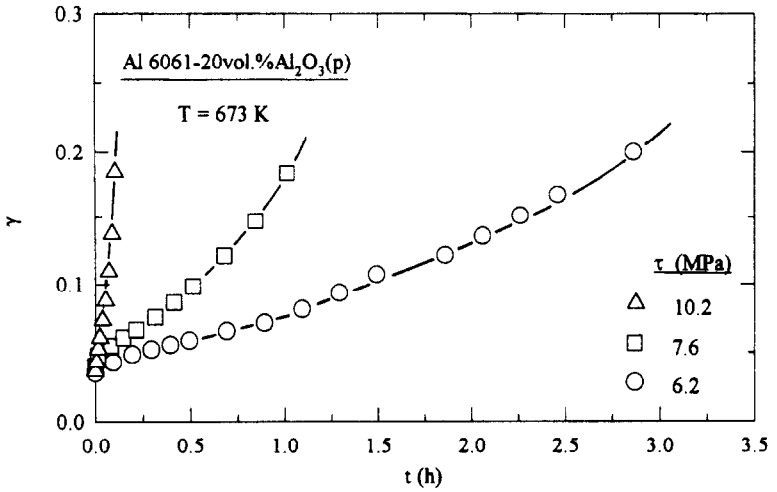

Fig. 2. Representative creep curves at a temperature of 673 K.

datum points below $\sim 10^{-4}\ s^{-1}$ at temperatures of 623 and 673 K) where the creep behavior exhibits the typical appearance of metal matrix composites with a tendency for the apparent stress exponent, n_a ($= \partial \ln \dot{\gamma} / \partial \ln \tau$), to increase as the applied stress decreases; and there is a region II (at shear strain rates above $\sim 10^{-4}\ s^{-1}$ for temperatures of 623 and 673 K) where the creep rates are exceptionally fast and therefore the values of n_a are anomalously large. In region I, the estimated values of n_a vary from ~ 4 to > 10 as the stress level decreases.

The results in Fig. 4 may be used to determine the apparent activation energy for creep, $Q_a [= -R \partial \ln \dot{\gamma} / \partial (1/T)]$, from a semi-logarithmic plot of $\dot{\gamma}$ vs $1/T$ at a constant level of applied stress. Figure 5 shows a plot for shear stresses of 4 and 10 MPa giving values for Q_a of ~ 275 and ~ 198 kJ/mol, respectively. The conclusion that Q_a decreases with increasing level of stress is consistent with data reported earlier by Park *et al.* [13] for Al 6061–30 vol.% SiC(p). The apparent activation energies estimated in this investigation are therefore significantly higher than the values either for self-diffusion in Al (~ 143.4 kJ/mol [21]) or for diffusion of Mg in Al (~ 130.5 kJ/mol [22]).

4. DISCUSSION

4.1. Creep behavior in Al 6061–20vol% Al_2O_3(p)

It is convenient to divide the data documented in Fig. 4 into the two regions denoted by I and II and to examine these regions separately.

4.1.1. Creep behavior in region I. The creep data in region I show the characteristic curvature associated with the presence of a threshold stress [13, 23–25]. To examine this possibility, threshold stresses were estimated using the linear extrapolation procedure in which $\dot{\gamma}^{1/n}$ is plotted against τ on linear axes and the data are extrapolated linearly to zero strain rate [26].

Taking values for the true stress exponent, n, of 3, 5 and 8, representing control by viscous glide [27, 28], high temperature climb [29] and a constant structure model [16, 30], respectively, Fig. 6(a)–(c) shows the relevant plots using all of the datum points obtained

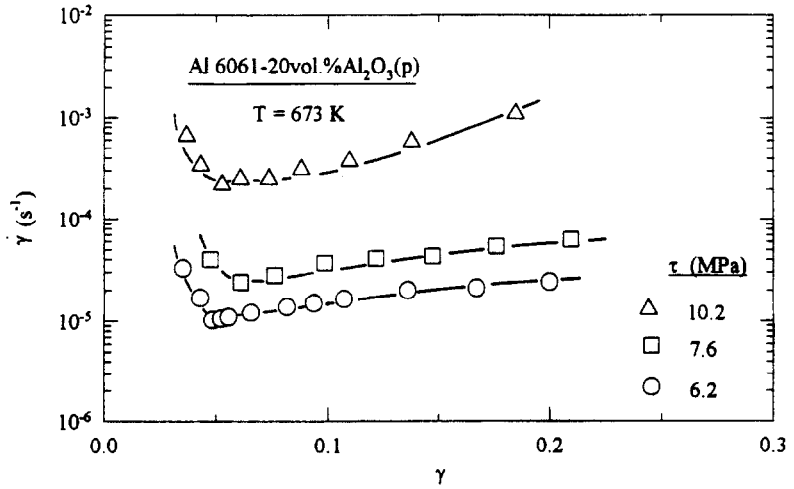

Fig. 3. Shear strain rate vs shear strain for the three specimens documented in Fig. 2.

in region I. Inspection reveals that there are marked curvatures in the plots of $\dot{\gamma}^{1/n}$ vs τ when using values for n of 5 and 8 but the plot with $n = 3$ gives an essentially linear correlation. By extrapolation of the straight lines in Fig. 6(a) to zero strain rate, the values of the threshold shear stress, τ_0, may be estimated at each testing temperature, as recorded in the central column in Table 1. Thus, as in other metal matrix composites [23, 31] and in dispersion strengthened alloys [32–37], the threshold stress in this material is a function of the testing temperature.

It is possible also to estimate the threshold stress using a new and simple procedure in which the creep data in a plot of strain rate vs stress are extrapolated to a lower limiting strain rate of 10^{-10} s^{-1} [38]. If the extrapolated lines are essentially vertical at this strain rate, and if the extrapolation takes place over no more than about two orders of magnitude of strain rate, it has been shown that the estimated threshold stresses are in good agreement with those obtained by the standard linear extrapolation method. The values of the threshold stresses estimated by this alternative approach are listed in the right-hand column of Table 1 and it is apparent that they are almost identical to those obtained by linear extrapolation using Fig. 6(a).

Using the threshold stresses obtained by the linear extrapolation method, Fig. 7 shows a logarithmic plot of $\dot{\gamma}$ vs the effective stress $(\tau - \tau_0)$. As anticipated, the creep data for each temperature provide a reasonable fit to a straight line with a true stress exponent of $n = 3$. This value of n is typical of solid solution alloys in which the viscous glide of dislocations is the rate-controlling process [27, 28] and it is consistent also with the estimated value of the true stress exponent for the Al 6061–20 vol.% Al_2O_3(s) composite [2].

When creep occurs in the presence of a threshold stress, the minimum or steady-state shear strain rate

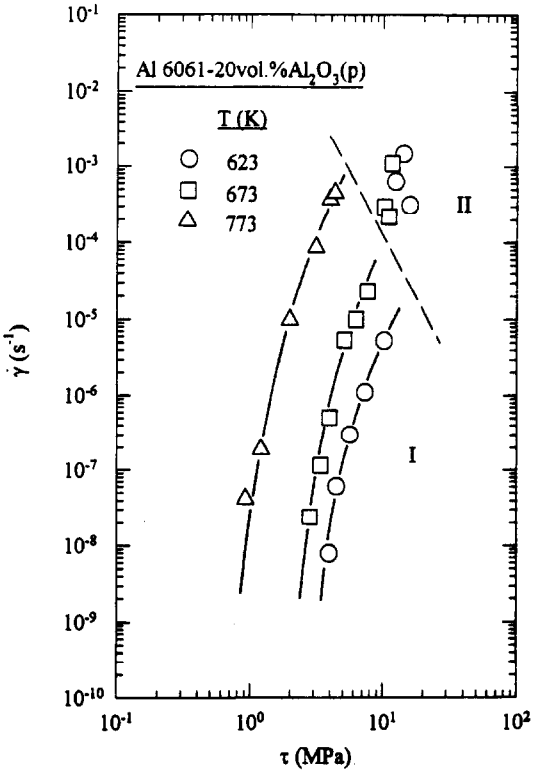

Fig. 4. Shear strain rate vs shear stress showing the division into regions I and II.

may be expressed in the form

$$\dot{\gamma} = \frac{ADGb}{kT}\left(\frac{\tau - \tau_0}{G}\right)^n \tag{1}$$

where D is the appropriate diffusion coefficient [$= D_0 \exp(-Q/RT)$, where D_0 is a frequency factor, Q is the true activation energy for creep and R is the gas constant], G is the shear modulus, b is the magnitude of the Burgers vector, k is Boltzmann's constant and A is a dimensionless constant. Therefore, taking

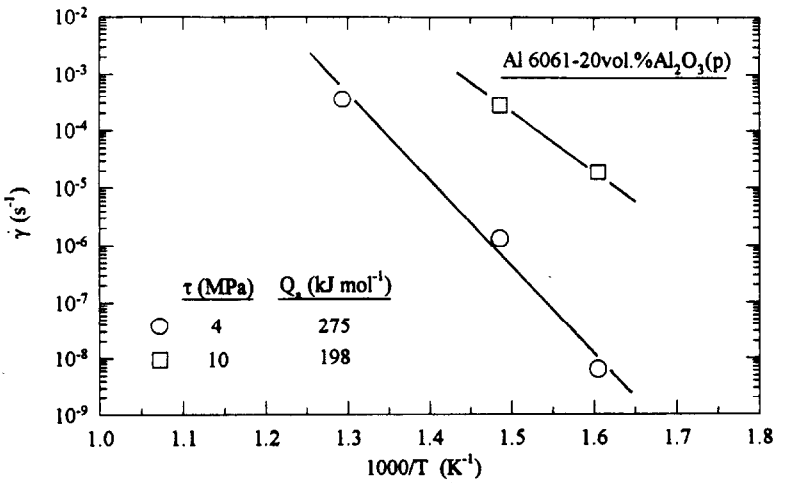

Fig. 5. Semi-logarithmic plot of shear strain rate vs the reciprocal of the absolute testing temperature for shear stresses of 4 and 10 MPa.

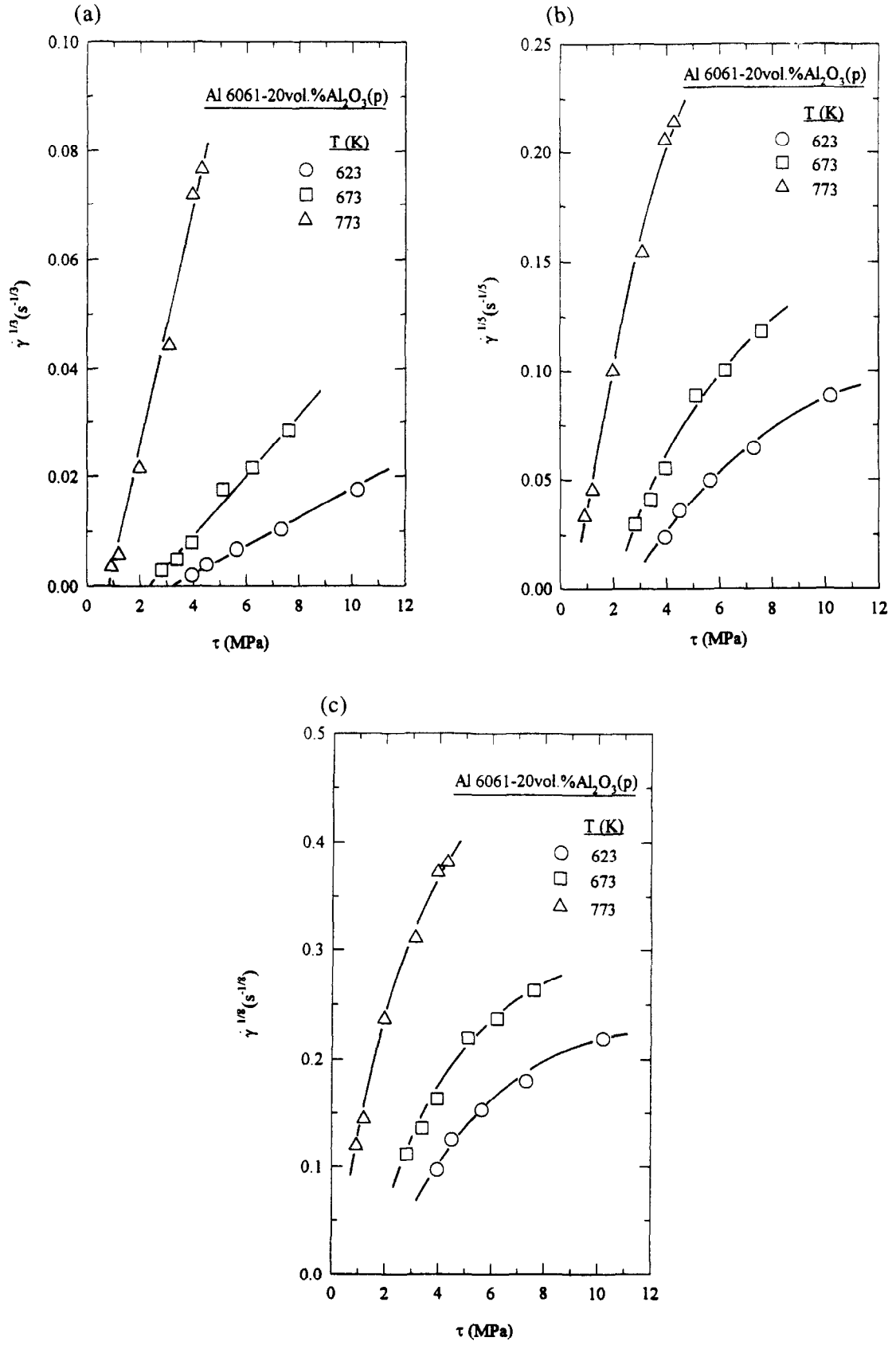

Fig. 6. The linear extrapolation method for estimating the threshold stresses using values for n of (a) 3, (b) 5 and (c) 8.

Table 1. Estimated values of the threshold stresses for creep

	τ_0 (MPa)	
T (K)	Linear extrapolation ($n = 3$)	Stress at $\dot{\gamma} = 10^{-10}$ s^{-1}
623	3.0	3.1
673	2.4	2.4
773	0.9	1.0

$n = 3$ from Fig. 7, it follows that the value of Q may be determined through a semi-logarithmic plot of $\dot{\gamma}G^{n-1}T$ ($= \dot{\gamma}G^2T$) vs $1/T$. This plot is shown in Fig.8 and leads to an activation energy for creep of $Q \simeq 150$ kJ/mol.

This value of Q is slightly higher than the activation energy for either self-diffusion in Al (143.4 kJ/mol) or diffusion of Mg atoms in Al (130.5 kJ/mol) and it is higher also than the value of $Q \simeq 125$ kJ/mol obtained in the Al 6061–20 vol.% Al_2O_3(s) composite after creep testing in tension in the temperature range of 473–673 K [2]. A possible reason for this discrepancy may lie in the advent of a partial dissolution of precipitates in the Al-6061 matrix alloy at the highest testing temperature. It was shown earlier that there is a complex precipitation sequence for age hardening in the Al-6061 matrix alloy and ageing for 8 h (2.88×10^4 s) at 448 K, as required in the T6 heat treatment, corresponds to a peak ageing condition [39]. The present creep experiments were conducted at temperatures up to $> 300°$ higher than the ageing temperature, thereby

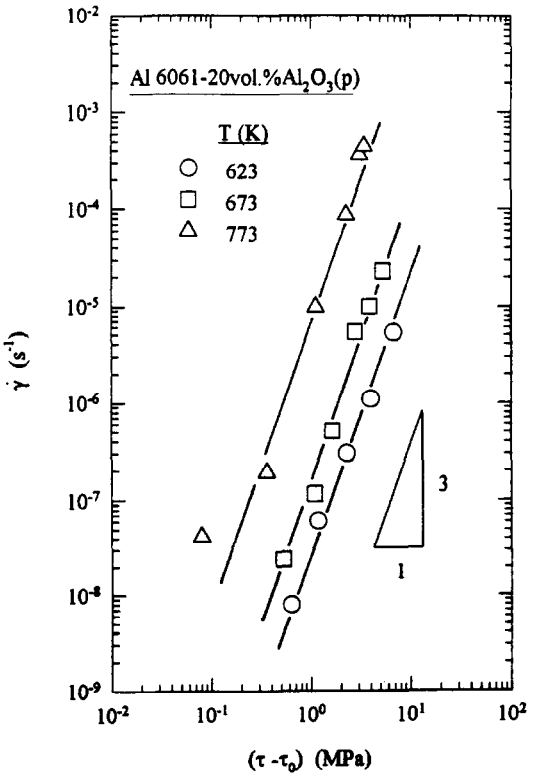

Fig. 7. Shear strain rate vs effective shear stress for creep data in region I.

introducing the possibility of partial dissolution of some precipitates and, consequently, a creep weakening and overestimation of Q. This suggestion is consistent with experimental data presented earlier showing a decrease in the strain hardening rate of the Al-6061 matrix alloy after a T6 heat treatment and subsequent compression testing at temperatures above ~ 625 K [1]. There is also direct experimental evidence, using differential scanning calorimetry on the Al-6061 matrix alloy, for an endothermic peak at ~ 810 K owing to dissolution of the β-Mg_2Si precipitates [40]. In addition, support for this proposal is provided by noting that if Q is estimated by considering only the two lowest temperatures in Fig. 7, where partial dissolution is probably not significant, the value of Q is reduced to ~ 130 kJ/mol which corresponds to the anticipated value for diffusion of Mg in Al [22].

Since the true stress exponent for creep is equal to 3, and the true activation energy for creep appears to be close to the value for interdiffusion of Mg in the Al matrix alloy, it is reasonable to conclude that creep of the Al 6061–20 vol.% Al_2O_3(p) composite in region I is controlled by the viscous glide of dislocations dragging Mg atom atmospheres. To check this conclusion, Fig. 9 shows a logarithmic plot of the normalized creep rate, $\dot{\gamma}kT/\tilde{D}Gb$, against the normalized effective stress, $(\tau - \tau_0)/G$, for those datum points given in Fig. 4 and lying within region I: this plot is constructed using the coefficient for diffusion of Mg in Al, $\tilde{D}$, given by [22]

$$\tilde{D} = 1.24 \times 10^{-4} \exp(-130.5/RT) \text{m}^2 \text{ s} \quad (2)$$

the shear modulus for pure Al (in MPa) defined as [41]

$$G = (3.022 \times 10^4) - (16T) \quad (3)$$

and $b = 2.86 \times 10^{-10}$ m for pure Al. It is apparent from Fig. 9 that the experimental data at 623 and 673 K are consistent with this interpretation but the datum points at 773 K are faster than anticipated, by a factor of ~ 3, because of the creep weakening associated with partial precipitate dissolution.

4.1.2. Creep behavior in region II. The experimental points in region II of Fig. 4 are significantly faster than anticipated by extrapolation of the lines in region I and therefore the stress exponent appears to be exceptionally high. Although a high stress exponent has been reported in several creep experiments on metal matrix composites [10, 12–14, 24, 42], this trend is generally observed either at low stresses because of the presence of a threshold stress [13, 24] or over the total stress range examined experimentally [10, 12, 14, 42]. Two possible explanations are available to account for a transition to a region having a high apparent stress exponent at high stress levels. First, the transition may arise from power-law breakdown such that the creep rate then has an exponential dependence upon stress [43]. Second, it may arise because the dislocations break

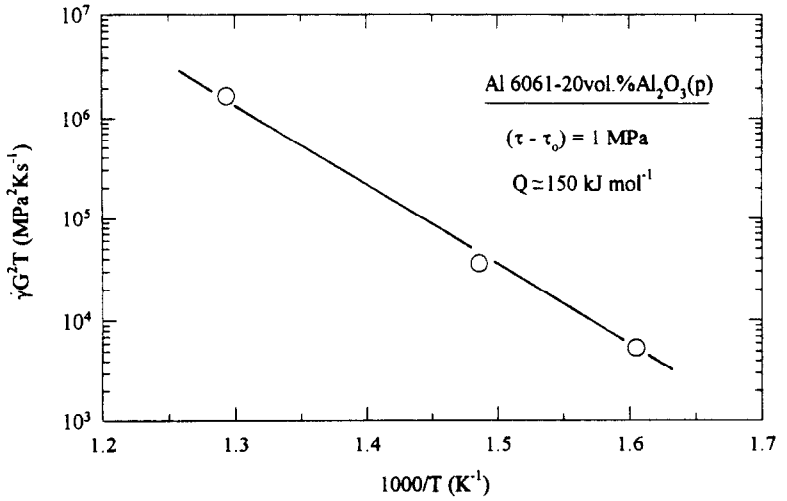

Fig. 8. Semi-logarithmic plot of $\dot{\gamma}G^2T$ vs $1/T$ in order to obtain the true activation energy for creep, Q.

away from their solute atom atmospheres [44, 45]. These two possibilities are now examined.

Sherby and Burke [46] demonstrated that power-law breakdown occurs in face-centered cubic (f.c.c) metals at a normalized strain rate of the order of $\dot{\epsilon}/D \approx 10^{13}\,\mathrm{m}^{-2}$ so that, for tests conducted under double-shear conditions, the upper limiting normalized shear strain rate for power-law creep is given by $\dot{\gamma}/D \simeq 1.5 \times 10^{13}\,\mathrm{m}^{-2}$. Considering, as an initial assumption, that creep occurs by the viscous glide process, and using the diffusion coefficient for diffusion of Mg atoms in Al given in equation (2), the limiting values of $\dot{\gamma}$ are estimated as $\sim 2 \times 10^{-2}$, $\sim 1 \times 10^{-1}$ and $\sim 3\,\mathrm{s}^{-1}$ for testing temperatures of 623, 673 and 773 K, respectively. Alternatively, if it is assumed instead that the creep occurs by high temperature climb controlled by lattice self-diffusion in Al, the diffusion coefficient, D_ℓ, is given by [21]

$$D_\ell = 1.86 \times 10^{-4}\exp(-143.4/RT)\mathrm{m}^2/\mathrm{s} \quad (4)$$

and the limiting values of $\dot{\gamma}$ are then estimated as $\sim 3 \times 10^{-3}$, $\sim 2 \times 10^{-2}$ and $\sim 6 \times 10^{-1}\,\mathrm{s}^{-1}$ for the same three testing temperatures, respectively. All of these estimated values for $\dot{\gamma}$, using both $\tilde{D}$ and D_ℓ in place of D, are significantly faster than the experimental datum points recorded in Fig. 4. Therefore, the advent of region II cannot be attributed to power-law breakdown.

It is well established that dislocations are capable of breaking away from their solute atmospheres at high stress levels, and the critical breaking stress, σ_c, may be expressed in a simple form as [47]

$$\sigma_c = \frac{W_m^2 c}{5b^3 kT} \quad (5)$$

where W_m is the binding energy between the solute atom and the dislocation and c is the concentration of the solute.† Thus, the solute atmospheres no longer retard the movement of dislocations at $\sigma > \sigma_c$. The binding energy, W_m, is given by [47]

$$W_m = -\frac{1}{2\pi}\left(\frac{1+\mu}{1-\mu}\right)G|\Delta V_a| \quad (6)$$

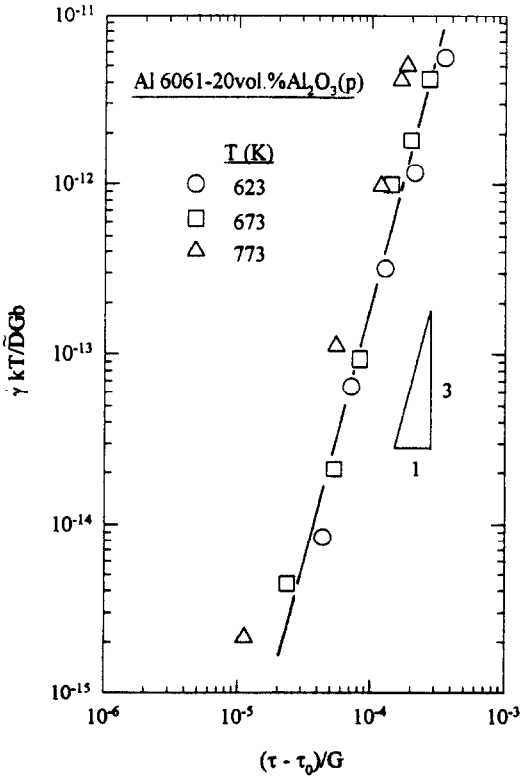

Fig. 9. Normalized shear strain rate vs normalized effective shear stress for creep data in region I.

†As noted elsewhere [45], equation (5) is a simplified expression which ignores both the variation in the interaction energy with solute concentration and the effect of the different spacings between the solute atoms and the dislocation line. In practice, it has been shown that equation (5) tends to overestimate σ_c by a factor of ~ 2 [45].

where μ is Poisson's ratio and ΔV_a is the difference in volume between the solute and the solvent atoms.

The value for c in equation (5) is governed by the concentration of ~ 1 wt% of Mg atoms in the Al-6061 matrix alloy, equivalent to ~ 1.1 at.% of Mg. Taking $\Delta V_a = 5.8 \times 10^{-30}$ m^3 [47] and $\mu = 0.34$, and with $\tau_c = \sigma_c/2$, the values of the critical break-away shear stresses, τ_c, are estimated as ~ 7.9, ~ 6.7 and ~ 5.0 MPa for testing temperatures of 623, 673 and 773 K, respectively. Now, taking into consideration the presence of a threshold stress, the transitions observed experimentally occur at shear stresses of ~ 7–9 and ~ 6–8 MPa for the two lowest testing temperatures of 623 and 673 K, respectively. These two values are therefore consistent with the stresses estimated from equation (5). No similar comparison is possible at the highest testing temperature of 773 K because the tests were then discontinued at an upper effective stress of 3.2 MPa and there was no evidence for a transition to region II.

From these calculations, it is reasonable to conclude that the points designated as region II in Fig. 4 lie above the critical stress at which the dislocations in the matrix alloy break away from their solute atom atmospheres.

4.2. *The threshold stress in the composite*

It is evident from Table 1 that the threshold stress decreases with increasing temperature. The normalized threshold stress, τ_0/G, is often represented by an expression of the form [31]

$$\frac{\tau_0}{G} = B \exp\left(\frac{Q_0}{RT}\right) \tag{7}$$

where B is a constant and Q_0 is an energy term which is associated with the binding between the dislocations and the obstacles giving rise to the threshold stress. Using the temperature dependence of the values of τ_0 obtained by the linear extrapolation method and listed in Table 1, Q_0 may be estimated as ~ 25 kJ/mol (equivalent to ~ 0.26 eV). This value of Q_0 is of the same order as the values of ~ 19.3 kJ/mol reported both for Al 6061–30 vol.% SiC(p) [31] and for an unreinforced 6061 PM Al alloy [48], ~ 23 kJ/mol reported for an unreinforced 2024 PM Al alloy [49] and ~ 21 kJ/mol reported for an unreinforced Al–Si–Ni–Cr alloy produced by rapid solidification processing [50].††

In the creep of dispersion strengthened materials, the threshold stress arises from the presence of a fine dispersion of stable incoherent particles. Several different models have been developed to account for the threshold stress including the Orowan stress for the bowing of dislocations between the particles [51], the back stress which is needed to create an additional segment of dislocation as it surmounts the obstacle by local climb [52, 53] and the detachment stress associated with detaching a dislocation from an attractive particle [54–56]. None of these models is appropriate in the present investigation because the Al_2O_3 particles have an average size of ~ 20 μm which is comparable with the grain size. Therefore, as is evident from inspection of Fig. 1, any model based on the bowing of dislocations between the particulate reinforcement is clearly unrealistic.

In Al-6061 matrix composites reinforced with SiC particles and produced using powder metallurgy processing, the threshold stress has been attributed to the presence of an array of fine incoherent oxide particles introduced into the matrix alloy during atomization in the fabrication process [13]. A similar explanation was given also to account for the threshold stresses observed in the creep of the unreinforced Al-6061 matrix alloy fabricated by a powder metallurgy technique [48]. It may appear initially that an explanation of this type cannot be used in the present experiments because the composite was fabricated using ingot metallurgy. Nevertheless, an examination by transmission electron microscopy of the liquid metallurgy Al 6061–20 vol.% Al_2O_3(s) composite revealed the presence of many fine spinel precipitates in the matrix alloy which was tentatively attributed to the occurrence of oxidation in the melt during processing [57]. In addition, it is well established that the Al-6061 matrix alloy contains a high density of β'' precipitates after ageing at the peak conditions [39] and these precipitates ultimately transform into incoherent platelets of equilibrium β-Mg_2Si precipitates by lateral coarsening [58]. Evidence was presented earlier demonstrating that the β'' precipitates grow during creep testing at a temperature of 573 K [1] but there are no comparable observations at the higher testing temperatures used in the present experiments. Thus, although the precise origin of the threshold stress in the Al 6061–20 vol.% Al_2O_3(p) composite cannot be identified unambiguously at the present time, it appears that a sufficient array of fine precipitates is available in the Al-6061 matrix alloy to introduce a threshold stress in a manner similar to the behavior of dispersion strengthened materials.

4.3. *A comparison with the creep of Al 6061–20vol% Al_2O_3(s)*

It is appropriate to compare the present results with the creep data reported earlier for a composite reinforced with Al_2O_3 microspheres [1, 2]. Both materials were produced using an Al-6061 matrix alloy and a liquid processing route. In addition, the two composites are nominally identical in several respects:

1. Both composites were reinforced with alumina having a volume fraction close to 20%.
2. The average size of the reinforcement in both composites is ~ 20 μm.

††The designation PM signifies fabrication by a powder metallurgy technique.

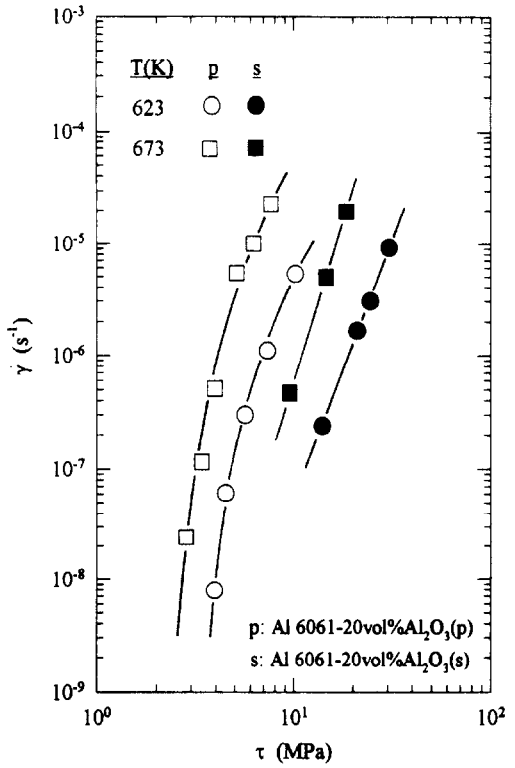

Fig. 10. Shear strain rate vs shear stress for Al-6061 metal matrix composites reinforced with 20 vol.% Al_2O_3 particulates (p) or 20 vol.% Al_2O_3 microspheres (s).

3. Both composites were subjected to an identical T6 heat treatment prior to creep testing.

The most significant difference between the two composites is that the present material was reinforced using irregularly shaped Al_2O_3 particles whereas in the earlier investigation the reinforcement was essentially spherical.

Figure 10 shows creep data for the two composites tested at the same temperatures of 623 and 673 K. It is clear that the values of the apparent stress exponents in both composites, as represented by the slopes of the plots given in Fig. 10, are essentially identical when compared over the same range of strain rate at the same testing temperature. Furthermore, both composites yield a true stress exponent close to 3 and an activation energy close to the value for diffusion of Mg in Al when the creep data are examined by incorporating a threshold stress into the analysis. It is therefore concluded that the rate-controlling creep mechanism in both composites is viscous glide of dislocations within the Al-6061 matrix alloy. Despite these similarities, however, the composite reinforced with microspheres exhibits creep rates which, at any selected stress level, are slower than the particulates reinforced composite by more than two orders of magnitude.

There are two possible explanations for the higher creep resistance in the Al 6061–20 vol.% Al_2O_3(s) composite. First, it may be associated with a higher dislocation density introduced into the matrix alloy of the composite reinforced with microspheres because of the CTE mismatch and a more effective dislocation generation using a spherical reinforcement. However, this explanation seems unlikely because, although there are no direct comparisons between composites reinforced with identical volume fractions of Al_2O_3, the dislocation density reported in the microsphere-reinforced composite in the as-quenched condition ($\sim 1.5 \times 10^{13}\,m^{-2}$ [39]) is consistent with the dislocation densities reported in a similar Al-6061 alloy reinforced with either 10 or 15 vol.% of irregularly shaped Al_2O_3 particulates ($\sim 4.5 \times 10^{12}$ and $\sim 7.3 \times 10^{12}\,m^{-2}$, respectively [40]). Second, the higher creep resistance may be a consequence of differences in the compositions of the Al_2O_3 reinforcements, thereby leading to different reaction products between the matrix and the reinforcement. This latter explanation is attractive because the microspheres consisted of a mixture of submicrometer grains of corundum (α-Al_2O_3) and mullite ($3Al_2O_3 \cdot 2SiO_2$) and with a significant amount of dissolved Fe, and there is good experimental evidence for an interfacial reaction between the microspheres and the aluminum melt leading to the formation of spinel ($MgAl_2O_4$) crystals and subsequently, upon cooling, to particles of the b.c.c. α-AlFeSi intermetallic [57, 59]. The observations suggest, therefore, that these Al-6061 composites reinforced with particulates or microspheres both contain arrays of fine precipitates which introduce a threshold stress into the creep behavior, but more precipitates are present in the microsphere-reinforced material, leading to a greater creep resistance, because of the additional products created in the interfacial reaction between the Al-6061 matrix alloy and the microsphere reinforcement.

5. SUMMARY AND CONCLUSIONS

1. Creep tests were conducted on an Al-6061 metal matrix composite fabricated using an ingot metallurgy technique and reinforced with 20 vol.% of irregularly shaped Al_2O_3 particulates.

2. For testing temperatures in the range from 623 to 773 K, high values were obtained for both the apparent stress exponent and the activation energy for creep.

3. By incorporating a threshold stress into the analysis, it is shown that the true stress exponent is close to 3 and the true activation energy is close to the value for diffusion of Mg in Al. Therefore, creep is controlled by the viscous glide of dislocations in the Al-6061 matrix.

4. Exceptionally rapid creep rates are observed at the highest stress levels and it is demonstrated that these high rates arise when the dislocations break away from their solute atom atmospheres.

5. A comparison shows that greater creep resistance is attained in an Al-6061 composite reinforced

with 20 vol.% of Al_2O_3 microspheres. This increase in creep resistance is attributed to the presence of additional precipitates which are created as a result of an interfacial reaction between the Al matrix and the microsphere reinforcement.

Acknowledgement—This work was supported by the U.S. Army Research Office under Grant DAAH04-96-1-0332.

REFERENCES

1. Furukawa, M., Wang, J., Horita, Z., Nemoto, M., Ma, Y. and Langdon, T. G., *Metall. Mater. Trans.*, 1995, **26A,** 633.
2. Ma, Y. and Langdon, T. G., *Mater. Sci. Engng*, in press.
3. Couper, M. J. and Xia, K., in *Metal Matrix Composites—Processing, Microstructure amd Properties*, ed. N. Hansen, D. Juul Jensen, T. Leffers, H. Lilholt, T. Lorentzen, A. S. Pedersen, O. B. Pederson and B. Ralph. Risø National Laboratory, Roskilde, Denmark, 1991, p. 291.
4. Arsenault, R. J. and Fisher, R. M., *Scripta metall.*, 1983, **17,** 67.
5. Nieh, T. G. and Karlak, R. F., *Scripta metall.*, 1984, **18,** 25.
6. Suresh, S., Christman, T. and Sugimura, Y., *Scripta metall.*, 1989, **23,** 1599.
7. Arsenault, R. J., Wang, L. and Feng, C. R., *Acta metall. mater.*, 1991, **39,** 47.
8. Taya, M., Lulay, K. E. and Lloyd, D. J. *Acta metall. mater.*, 1991, **39,** 73.
9. Vogelsang, M., Arsenault, R. J. and Fisher, R. M., *Metall, Trans.*, 1986, **17A,** 379.
10. Nieh, T. G., Xia, K. and Langdon, T. G., *J. Engng Mater. Technol.*, 1988, **110,** 77.
11. Webster, D., *Metall. Trans.*, 1982, **13A,** 1511.
12. Nieh, T. G., *Metall. Trans.*, 1984, **15A,** 139.
13. Park, K.-T., Lavernia, E. J. and Mohamed, F. A., *Acta metall. mater.*, 1990, 38, 2149.
14. Xia, K., Nieh, T. G., Wadsworth, J. and Langdon, T. G., in *Fundamental Relationships Between Microstructure and Mechanical Properties of Metal-Matrix Composites*, ed. P. K. Liaw and M. N. Gungor. The Minerals, Metals and Materials Society, Warrendale, PA, 1990, p. 543.
15. Pandey, A. B., Mishra, R. S. and Mahajan, Y. R., *Acta metall. mater.*, 1992, **40,** 2045.
16. González-Doncel, G. and Sherby, O. D., *Acta metall. mater.*, 1993, **41,** 2797.
17. Morimoto, T., Yamaoka, T., Lilholt, H. and Taya, M., *J. Engng Mater. Technol.*, 1988, **110,** 70.
18. Dragone, T. L. and Nix, W. D., *Acta metall. mater.*, 1992, **40,** 2781.
19. Chirouze, B. Y., Schwartz, D. M. and Dorn, J. E., *Trans. Q. Am. Soc. Metals*, 1967, **60,** 51.
20. Murty, K. L., Mohamed, F. A. and Dorn, J. E., *Acta metall.*, 1972, **20,** 1009.
21. Mohamed, F. A. and Langdon, T. G., *Metall. Trans.*, 1974, **5,** 2339.
22. Rothman, S. J., Peterson, N. L., Nowicki, L. J. and Robinson, L. C., *Phys. stat. solidi (b)*, 1974, **63,** K29.
23. Čadek, J., Oikawa, H, Šustek, V. and Pahutová, M., *High Temp. Mater. Prop.*, 1994, **13,** 327.
24. Čadek, J. and Šustek, V., *Scripta metall. mater.*, 1994, **30,** 277.
25. Čadek, J., Oikawa, H. and Šustek, V., *Mater. Sci. Engng*, 1995, **A190,** 9.
26. Lagneborg, R. and Bergman, B., *Metal Sci.*, 1976, **10,** 20.
27. Weertman, J., *J. appl. Phys.*, 1957, **28,** 1185.
28. Mohamed, F. A. and Langdon, T. G., *Acta metall.*, 1974, **22,** 779.
29. Weertman, J., *J. appl. Phys.*, 1957, **28,** 362.
30. Sherby, O. D., Klundt, R. H. and Miller, A. K., *Metall. Trans.*, 1977, **8A,** 843.
31. Mohamed, F. A., Park, K.-T. and Lavernia, E. J., *Mater. Sci. Engng*, 1992, **A150,** 21.
32. Howson, T. E., Mervyn, D. A. and Tien, J. K., *Metall. Trans.*, 1980, **11A,** 1599.
33. Howson, T. E., Mervyn, D. A. and Tien, J. K., *Metall. Trans.*, 1980, **11A,** 1609.
34. Clauer, A. H. and Hansen, N., *Acta metall.*, 1984, **32,** 269.
35. Kucharová, K., Orlová, A., Oikawa, H. and Čadek, J., *Mater. Sci. Engng*, 1988, **A102,** 201.
36. Yeh, Y. H., Nakashima, H., Kurishita, H. and Yoshinaga, H., *Mater. Trans. JIM*, 1990, **31,** 284.
37. Mishra, R. S., Paradkar, A. G. and Rao, K. N., *Acta metall. mater.*, 1993, **42,** 2243.
38. Li, Y. and Langdon, T. G., *Scripta mater.*, 1997, **36,** 1457.
39. Wang, J., Furukawa, M., Horita, Z., Nemoto, M., Ma, Y. and Langdon, T. G., *Metall. Mater. Trans.*, 1995, **26A,** 581.
40. Dutta, I., Allen, S. M. and Hafley, J. L., *Metall. Trans.*, 1991, **22A,** 2553.
41. Yavari, P., Mohamed, F. A. and Langdon, T. G., *Acta metall.*, 1981, **29,** 1495.
42. Nardone, V. C. and Strife, J. R., *Metall. Trans.*, 1987, **18A,** 109.
43. Nix, W. D. and Ilschner, B., in *Strength of Metals and Alloys (ICSMA 5)*, Vol. 3, ed. P. Haasen, V. Gerold and G. Kostorz. Pergamon, Oxford, 1980, p. 1503.
44. Yavari, P. and Langdon, T. G., *Acta metall.*, 1982, **30,** 2181.
45. Endo, T., Shimada, T. and Langdon, T. G., *Acta metall.*, 1984, **32,** 1991.
46. Sherby, O. D. and Burke, P. M., *Prog. Mater. Sci.*, 1967, **13,** 325.
47. Friedel, J., *Dislocations*. Pergamon, Oxford, 1964.
48. Park, K.-T., Lavernia, E. J. and Mohamed, F. A., *Acta metall. mater.*, 1994, **42,** 667.
49. Kloc, L., Spigarelli S., Cerri, E., Evangelista, E. and Langdon, T. G., *Acta mater.*, 1997, **45,** 529.
50. Kloc, L., Spigarelli S., Cerri, C., Evangelista, E. and Langdon, T. G., *Metall. Mater. Trans.*, 1996, **27A,** 3871.
51. Orowan, E., in *Dislocations in Metals*, ed. M. Cohen. AIME, New York, 1954, p. 131.
52. Shewfelt, R. S. W. and Brown, L. M., *Phil. Mag.*, 1977, **35,** 945.
53. Arzt, E. and Ashby, M. F., *Scripta metall.*, 1982, **16,** 1285.
54. Arzt, E. and Wilkinson, D. S., *Acta metall.*, 1986, **34,** 1893.
55. Arzt, E. and Rösler, J., *Acta metall.*, 1988, **36,** 1053.
56. Rösler, J. and Arzt, E., *Acta metall.*, 1990, **38,** 671.
57. Drennan, J., Xia, K. and Couper, M. J. in *Advanced Composites '93*, ed. T. Chandra and A. K. Dhingra. The Minerals, Metals and Materials Society, Warrendale, PA, 1993, p. 1015.
58. Dutta, I. and Allen, S. M., *J. Mater. Sci. Lett.*, 1991, **10,** 323.
59. Yao, J. Y., Edwards, G. A., Couper, M. J. and Dunlop, G. L., in *Aluminium Alloys: Their Physical and Mechanical Properties (ICAA3)*, Vol. 1, ed. L. Amberg, O. Lohne, E. Nes and N. Ryum. The Norwegian Institute of Technology, Trondheim, Norway, 1992, p. 429.